

Sparse Aperture Masking Observations of the FL Cha Pre-transitional Disk

Lucas A. Cieza^{1,9}, Sylvestre Lacour², Matthias R. Schreiber^{3,10}, Simon Casassus^{4,10}, Andrés Jordán^{5,10}, Geoffrey S. Mathews¹, Héctor Cánovas^{3,10}, François Ménard^{6,10}, Adam L. Kraus^{1,11}, Sebastián Pérez⁴, Peter Tuthill⁷, and Michael J. Ireland⁸

ABSTRACT

We present deep Sparse Aperture Masking (SAM) observations obtained with the ESO Very Large Telescope of the pre-transitional disk object FL Cha (SpT=K8, $d=160$ pc), the disk of which is known to have a wide optically thin gap separating optically thick inner and outer disk components. We find non-zero closure phases, indicating a significant flux asymmetry in the K_S -band emission (e.g., a departure from a single point source detection). We also present radiative transfer modeling of the SED of the FL Cha system and find that the gap extends from $0.06^{+0.05}_{-0.01}$ AU to 8.3 ± 1.3 AU. We demonstrate that the non-zero closure phases can be explained

¹Institute for Astronomy, University of Hawaii at Manoa, Honolulu, HI 96822, USA

²LESIA, CNRS/UMR-8109, Observatoire de Paris, UPMC, Université Paris Diderot, 5 place Jules Janssen, 92195, Meudon, France

³Departamento de Física y Astronomía, Universidad de Valparaíso, Valparaíso, Chile

⁴Departamento de Astronomía, Universidad de Chile, Camino del Observatorio 1515, Las Condes, Santiago, Chile

⁵Departamento de Astronomía y Astrofísica, Pontificia Universidad Católica de Chile, 7820436 Macul, Santiago, Chile

⁶UMI-FCA, CNRS / INSU France (UMI 3386)

⁷School of Physics, University of Sydney, NSW 2006, Australia

⁸Department of Physics and Astronomy, Macquarie University, NSW 2109, Australia

⁹ *Sagan* Fellow, lcieza@ifa.hawaii.edu

¹⁰Millennium Nucleus “Protoplanetary Disks in ALMA Early Science”, Universidad de Chile, Casilla 36-D, Santiago, Chile

¹¹ *Hubble* Fellow

almost equally well by starlight scattered off the inner edge of the *outer* disk or by a (sub)stellar companion. Single-epoch, single-wavelength SAM observations of transitional disks with large cavities that could become resolved should thus be interpreted with caution, taking the disk and its properties into consideration. In the context of a binary model, the signal is most consistent with a high-contrast ($\Delta K_S \sim 4.8$ mag) source at a ~ 40 mas (6 AU) projected separation. However, the flux ratio and separation parameters remain highly degenerate and a much brighter source ($\Delta K_S \sim 1$ mag) at 15 mas (2.4 AU) can also reproduce the signal. Second-epoch, multi-wavelength observations are needed to establish the nature of the SAM detection in FL Cha.

Subject headings: circumstellar matter — protoplanetary disks — stars: individual (FL Cha) — planetary systems — techniques: interferometric

1. Introduction

Primordial circumstellar disks with inner cavities or gaps are known as “transitional” disks and can be identified by their peculiar Spectral Energy Distributions (SEDs), which have reduced levels of near- and/or mid-IR excesses with respect to the vast majority of Classical T Tauri star (CTTS) disks. Nevertheless, not all transitional disk SEDs look the same and it is clear that not all inner holes and gaps are produced in the same way. Grain-growth, photoevaporation, and dynamical interactions with (sub)stellar companions can all result in transitional disk SEDs (see Williams & Cieza, 2011, for a recent review). Distinguishing between the processes that could be responsible for the unusual SEDs of transitional disks requires considerable information: SED shapes, accretion rates, disk masses, and multiplicity information (Najita et al. 2007).

FL Cha belongs to a subclass of transitional objects known as “pre-transitional” disks, which is characterized by a pronounced “dip” in the mid-IR SED (Espaillat et al. 2007). The SEDs of pre-transitional disks can be reproduced with models presenting a wide (>5 - 10 AU) optically thin gap separating an optically thick inner disk from an optically thick outer disk. The inner and the outer disk components of pre-transitional objects have already been resolved by long-baseline interferometry observations in the near-IR (e.g., Olofsson et al. 2011; Tatulli et al. 2011) and the submillimeter (e.g., Andrews et al. 2011), respectively, confirming the gapped structure. These gaps are not necessarily empty. Deep polarized intensity images reveal a population of μm -sized grains within some of the gaps (Dong et al. 2012) and the accretion rates onto the stars in pre-transitional systems suggest that the inner disks are continuously replenished with material from the outer disks. Since pre-transitional

disks tend to lack stellar companions (Pott et al. 2010; Kraus et al. 2011), their gaps are best explained by the dynamical interaction of unseen substellar or planetary-mass objects embedded in the disk (Dobson-Robinson & Salyk, 2012). Recent high-contrast observations using the Sparse Aperture Masking (SAM) interferometric technique on Keck and the VLT have already identified companion candidates to two other pre-transitional disks, T Cha (Huélamo et al. 2011) and LkCa 15 (Kraus & Ireland, 2012).

FL Cha is a K8 CTTS (Luhman 2007) in the Chamaeleon I molecular cloud, located at 160 pc (Whittet et al. 1997). As part of a program aiming the direct detection of young planets in transitional disks (see also Schreiber et al. 2013), we have obtained deep VLT-SAM observations of FL Cha. Our SAM data show non-zero closure phases indicating a second source of near-IR emission besides the central star. We also present radiative transfer modeling of the FL Cha SED, in order to better constrain the size of the gap, and discuss the possible nature of the newly identified source.

2. SAM observations and data analysis

2.1. Observations

The VLT-SAM observations of FL Cha were performed on March 6, 2012, using the “7-hole” mask (Tuthill et al. 2010) on the NAOS-CONICA (NaCo) Adaptive Optics system (Lenzen et al. 2003). The mask at the pupil-plane blocks most of the light from target and resamples the primary mirror into a set of smaller sub-apertures that form a sparse interferometric array with 21 baselines. SAM observations allow for exquisite calibration of the point spread function of the stellar primary and the suppression of speckle noise by the application of interferometric analysis techniques, such as the measurement of closure phases (the sum of the phases around any 3 triangle of baselines). The SAM technique is sensitive to companions in the $\sim 0.5\text{-}5 \lambda/D$ separation range (corresponding to $\sim 30\text{-}300$ mas for K_S -band observations in the VLT) and can reach a contrast limit of $\Delta K \sim 7$ mag at λ/D (Kraus & Ireland, 2012).

The observing sequence consisted of multiple “visits” (4 observations of 25 frames of 10 s in K_S -band) of FL Cha, alternating with observations of the stars FI Cha, FK Cha, and 2MASS J11082577-7648315 used as calibrators. During the same observing run, we also observed the close binary system RX J1106.3-7721 (Lafrenière et al. 2008) in the L' -band to validate our observing strategy and data reduction technique. The observations were reduced using the Paris SAMP pipeline as described by Lacour et al. (2011). Both FL Cha and RX J1106.3-7721 show non-zero closure phases, indicting a departure from a single

point-source detection (see Figure 1).

2.2. Binary model

In order to constrain the properties of the SAM detections, we first performed a Monte Carlo Markov Chain analysis using a simple binary model with 3 basic parameters: two positional parameters, either separation and position angle (PA) or ΔRA and Δdec , and the magnitude difference (Δm). The χ^2 maps of such models are shown in Figure 1 for both FL Cha and RX J1106.3-7721. Our procedure is identical to the one used by Schreiber et al. (2013). We find that the binary parameters for the RX J1106.3-7721 system are *very* well constrained by our observations and robust to the choice of priors (see Figure 2). The flux asymmetry signal in the closure phases of FL Cha is much weaker and results in much larger uncertainties in the model-derived parameters. While the PA is relatively well constrained, Δm and separation remain degenerate and highly dependent on the choice of prior distributions. This is illustrated in Figure 2, where we show the posteriori probability distributions for two different sets of priors: 1) uniform distributions for ΔRA , Δdec , and Δm and 2) uniform distributions for PA, Δm , and the logarithm of the separation. The data favors a $\Delta\text{m} \sim 4.8$ mag source, but there is a long tail in the probability distribution extending to lower Δm values. The posteriori distribution of the separation could be bimodal or unimodal depending on the adopted prior. The degeneracy between the Δm and separation parameters is a known problem for small separations ($\lesssim \lambda/D$) in aperture masking observations (Pravdo et al. 2006, Martinache et al. 2009) and is clearly seen in the joint distributions shown in Figure 2. The complex χ^2 surfaces in the joint distributions are consistent with two families of solutions: a relative bright source ($\Delta\text{K} \sim 1\text{-}3$ mag) at ~ 15 mas (2.4 AU) and a much fainter one ($\Delta\text{K} \sim 4\text{-}5$ mag) at $\sim 30\text{-}40$ mas (5.0-6.5 AU). The relative probability of these two solutions strongly depends on the choice of prior and can not be unambiguously estimated with the available data. Future H-band observations should provide the additional resolution needed to break the Δm -separation degeneracy and solve the two-solution ambiguity in the context of the binary model (see Schreiber et al. 2013).

3. Disk model

Espaillet et al. (2011) successfully reproduced the optical to $38 \mu\text{m}$ SED of FL Cha adopting a simple model consisting of two vertical walls: one inner wall at the dust sublimation distance of 0.04 AU that is responsible for the near-IR excess and an outer wall at 15 AU that reproduces the observed mid-IR excess. Here we use a more physical model

in order to provide further constraints on the size and location of the gap in the disk. We include photometry data at longer wavelengths (70 and 870 μm), which are sensitive to the properties of the outer disk.

3.1. Spectral energy distribution

We constructed the FL Cha SED from the sources listed in Table 1. We have also obtained 870 μm photometry with the Atacama Pathfinder Experiment (APEX) using the LABOCA camera (Siringo et al. 2009). The observations were executed on July 24, 2012 using the “wobbler on-off” mode and reduced with the standard bolometer array data analysis package BoA¹. FL Cha was detected with a signal to noise ratio of 12. The SED of FL Cha is also well sampled by a *Spitzer*-IRS spectrum covering the 5.2 to 38 μm region (Astronomical Observation Request #12696320). The 0.44 to 870 μm SED is shown in Figure 3. The optical and near-IR wavelengths were corrected by extinction, adopting $A_V = 3.14$ mag (calculated from the R_C - I_C color excess) and the extinction relations listed in Cieza et al. (2007). The median SED of CTTSs from Furlan et al. (2006) is shown for comparison. The sharp “dip” in the FL Cha SED around 15 μm indicates the presence of a wide gap in the disk.

3.2. Radiative transfer modeling

We model the observed SED using the Monte Carlo radiative transfer code MCFOST (Pinte et al. 2006). We parameterize the structure of the FL Cha disk with two independent components, an inner and an outer disk. Each component is described by the following parameters: the inner and outer radii (R_{in} and R_{out} , respectively) and the index γ for the surface density profile ($\Sigma(r) = \Sigma_{10}(r/10 \text{ AU})^\gamma$). The scale height as a function of radius is given by $H(r) = H_{10}(r/10 \text{ AU})^\psi$. The grain size distribution has the form $dn(a) \propto a^p da$, between the minimum (a_{min}) and maximum (a_{max}) grain sizes. The width of the gap in the disk is simply given by: $R_{outer,in} - R_{inner,out}$. The parameters a_{min} , a_{max} , p , ψ , γ , and $R_{outer,out}$, and the disk inclination are not easily constrained by the available data. We thus fix them to more or less “standard” values, which are listed in Table 2: For the dust composition, we follow Espaillat et al. (2011) and adopt a 40%/60% mixture of amorphous and crystalline silicates.

¹<http://www.apex-telescope.org/bolometer/laboca/boa/>

We adopt the fitting procedure described by Mathews et al. (2012), which uses the Levenberg-Marquardt χ^2 minimization algorithm to calculate the numerical gradients of the χ^2 function and determine the next point in the parameter space to be sampled until the algorithm converges to a χ^2 minimum. We ran the search algorithm 10 times using different starting values to better sample the parameter space. Each of the runs results in a set of best-fit parameters, the distribution of which can be used to calculate the mean and associated uncertainty.

The results of the 10 runs are listed in Table 2 and the structure of our best-fit model is shown in Figure 3. We find that the near-IR excess is best reproduced by a very narrow ring at the dust sublimation radius, extending from 0.04 to 0.06 AU, in agreement with the modeling results by Espaillat et al (2011). We also find that inner disks wider than ~ 0.1 AU significantly overproduce the observed near-IR fluxes and that the dip characteristic of pre-transitional disk SEDs disappears for inner disks wider than ~ 3 AU (for the given $R_{outer,in}$ value, resulting in gaps narrower than ~ 5 AU). In our model, the inner edge of the outer disk is located at 8.3 ± 1.3 AU from the star. This distance is a factor of ~ 2 smaller than that estimated by Espaillat et al. The source of the discrepancy is unclear, but since our models share the same stellar parameters, it is likely to be related to the different parametrizations used for the disk structure (two vertical walls versus a full 3-D disk model) and the different grain size distributions adopted. Resolved submillimeter images with ALMA should be able to directly measure the cavity size and settle the discrepancy. Our SED model also constrains the properties of the outer disk. In particular, we find the FL Cha disk is relatively “typical”, with a mass of $7.5 M_{JUP}$ and a scale height of ~ 1 AU at a radius of 10 AU.

4. Possible interpretations of the SAM detection

4.1. Background contamination

The probability $P(\Theta, m)$ for an unrelated source to be located within a certain angular distance Θ from a particular target is given by $P(\Theta, m) = 1 - e^{-\pi\rho(m)\Theta^2}$, where $\rho(m)$ is the cumulative surface density of background sources down to a limiting magnitude m (Brandner et al. 2000). FL Cha is 9.11 mag in K_S -band. Therefore, the peak in the ΔK_S probability distribution correspond to an apparent K_S -band magnitude of ~ 13.9 . Since there are 7482 stars brighter than $K_S = 13.9$ mag within a 1 deg radius of FL Cha in the *2MASS* catalog, the probability of a background source at a $\lesssim 0.050''$ separation is of the order of 5×10^{-6} . Background contamination can thus be discarded as a likely explanation for our SAM detection.

4.2. A stellar companion

In Section 2.2, we found the SAM data is consistent with both a relative bright source ($\Delta K \sim 1-3$ mag) at a projected separation of ~ 2.4 AU or a much fainter one ($\Delta K \sim 4-5$ mag) at $\sim 5.0-6.5$ AU. Evolutionary tracks of young low-mass objects are *very* uncertain, but can be used to address the nature of the putative companion and try to distinguish between a low-mass star, a brown dwarf, or a planet. According to the evolutionary tracks by Siess et al. (2000), FL Cha is a $0.6 M_{\odot}$ star and the former solution corresponds to a stellar companion with a mass in the $\lesssim 0.1-0.3 M_{\odot}$ range. In the recent radial velocity (RV) monitoring study of Chamaeleon I objects performed by Nguyen et al. (2012), FL Cha showed a constant RV (16.9 ± 1.1 km/s), close to the typical values in the region ($\sim 15.3 \pm 2$ km/s), over the 1 month baseline of the study. While the precision and time baseline of the measurements are clearly not enough to rule out most stellar binaries, the RV measurements disfavor solutions with stellar companions at ~ 2.4 AU. As a reference, a $0.1 M_{\odot}$ companion to a $0.6 M_{\odot}$ star with circular edge-on orbit and a 2.4 AU semi-major axis has a period of 4.46 years and a velocity amplitude of ± 2.5 km/sec.

4.3. A brown dwarf or a protoplanet

We now consider the nature of the source if ΔK_G is close to the ~ 4.8 mag peak shown in the probability distributions from Figure 2. This peak corresponds to an absolute magnitude of ~ 7.9 at 160 pc. This renders our source a factor of 3 brighter than the protoplanet candidate identified by Kraus & Ireland (2012) within the gap of the LkCa 15 disk, and the “hot start” models by Chabrier et al. (2000) assign it a mass of $\sim 15-20 M_{JUP}$, for an age of 1 Myr. Taken at face value, this would place the object at the bottom of the brown dwarf mass function. However, since the source seems to be located inside the gap of an accreting transitional disk, the inner disk of which is mostly depleted, it is reasonable to expect material from the outer disk to flow across the gap onto the inner disk and then the star. Under such circumstances, the low-mass object inside the gap should accrete most of the material being transported across the outer disk (Lubow & D’Angelo, 2006), resulting in significant accretion luminosity. SAM observations in H- and L-band would provide near-IR colors and help establishing whether the FL Cha detection is consistent with a brown dwarf or an actively accreting protoplanet surrounded by a disk, as seems to be the case in the LkCa 15 system.

4.4. Thermal emission or starlight scattered off the disk

Our SAM detection is inconsistent with direct thermal emission from the *inner* disk. Our radiative transfer model suggests that the inner disk is $\lesssim 1$ mas in diameter and the thermal contribution from the outer disk to the observed K-band flux is $< 0.01\%$. However, starlight scattered off the inner edge of the *outer* disk can in principle produce the observed signal. If the disk is highly inclined, the brightness of the projected rim would be asymmetric and could result in non-zero closure phases. To test this hypothesis, we generated a $2.2 \mu\text{m}$ ray traced image of the best-fit MCFOST model described in Section 3 and calculated the closure phases of the resulting image as seen at different position angles and inclinations (Figure 3). We find that a disk inclined by ~ 60 deg from face-on with a position angle² of ~ 150 deg results in closure phases that fit the SAM data almost as well as the best-fit binary model described in Section 2.2 does ($\chi^2 \sim 140$ vs. ~ 130). The difference in the χ^2 results is mostly due to the fact that the disk model produces slightly smaller phase values compared to both the binary model and the SAM data. However, we emphasize that the $2.2 \mu\text{m}$ model image depends on disk properties that are poorly constrained, such as the grain size distribution, the dust composition, and the detailed structure of both the inner and the outer disk. These disks parameters could be varied to improve the fit further. Pending more constraints (i.e., resolved images), the current model suffices to show that a disk (which also fits the SED) can produce the necessary closure phase signal. This demonstrates that *the circumstellar disk must be taken into consideration when interpreting SAM data of transitional disks with inner cavities that are large enough to become resolved*. High-resolution submillimeter imaging with ALMA would reveal the exact orientation and size of the cavity in the FL Cha disk. Such imaging should establish whether our SAM detection is in fact consistent with starlight scattered off the disk or, on the contrary, if the source is located well inside the hole, as in the case of the LkCa 15 system. Measuring the K_S -H and K_S -L colors of the source would also help testing the scattered light hypothesis. Looking for orbital motion from multi-epoch SAM observations should provide the ultimate test to distinguish between a companion and the scattered light scenario.

5. Summary and Conclusions

From VLT-SAM observations, we have identified a near-IR flux asymmetry in the pre-transitional object FL Cha. By modeling its SED, we find that the gap in its disks extends

²The position angle is the direction defined by the intersection between the plane of the disk and the plane of the sky.

from $0.06_{-0.01}^{+0.05}$ AU to 8.3 ± 1.3 AU. We have considered several potential possibilities for the nature of the source: a low-mass star, a brown dwarf, a protoplanet, thermal emission or starlight scattered off the disk, or a background object. Only direct thermal emission from the inner disk and background contamination can be ruled out. We find that light scattered off the inner edge of the *outer* disk can result in closure phases that fit the SAM data almost as well as binary models do. Single-epoch, single-filter SAM observations of transitional disks should thus be interpreted very cautiously, taking the disk into consideration. In the context of a binary model, the closure phases are most consistent with a $\Delta K_S \sim 4.8$ mag source at a 6 AU projected separation, but a much brighter one ($\Delta K_S \sim 1$ mag) at 2.4 AU can also reproduce the signal. H- and L-band SAM observations of FL Cha are highly desirable to 1) test for orbital motion, 2) break the current degeneracy between Δmag and separation in the binary model, and 3) provide near-IR colors to help distinguishing between the possible explanations. Resolved submillimeter images with ALMA are needed to establish the orientation of the system and provide a *direct* measurement of the inner cavity size to test the scattered light hypothesis and to better constrain the properties of the outer disk.

L.A.C was supported by NASA through the *Sagan* Fellowship Program. M.R.S., A.J., S.C., and F.M. acknowledge support from the Millenium Science Initiative, Chilean Ministry of Economy, Nucleus P10-022-F. G.S.M. acknowledges NASA/JPL funding support through grant RSA-1369686. A.L.K. was supported by NASA through the *Hubble* Fellowship program.

REFERENCES

- Andrews, S. M., Rosenfeld, K. A., Wilner, D. J., & Bremer, M. 2011, ApJ, 742, L5
- Brandner, W., Zinnecker, H., Alcalá, J. M., et al. 2000, AJ, 120, 950
- Chabrier, G., Baraffe, I., Allard, F., & Hauschildt, P. 2000, ApJ, 542, 464
- Cieza, L., Padgett, D. L., Stapelfeldt, K. R., et al. 2007, ApJ, 667, 308
- Cieza, L. A., Padgett, D. L., Allen, L. E., et al. 2009, ApJ, 696, L84
- Cieza, L. A., Schreiber, M. R., Romero, G. A., et al. 2012, ApJ, 750, 157
- Dodson-Robinson, S. E., & Salyk, C. 2011, ApJ, 738, 131
- Dong, R., Rafikov, R., Zhu, Z., et al. 2012, ApJ, 750, 161

- Espaillat, C., Calvet, N., D'Alessio, P., et al. 2007, *ApJ*, 670, L135
- Espaillat, C., Furlan, E., D'Alessio, P., et al. 2011, *ApJ*, 728, 49
- Furlan, E., Hartmann, L., Calvet, N., et al. 2006, *ApJS*, 165, 568
- Gauvin, L. S., & Strom, K. M. 1992, *ApJ*, 385, 217
- Guenther, E. W., Esposito, M., Mundt, R., et al. 2007, *A&A*, 467, 1147
- Huélamo, N., Lacour, S., Tuthill, P., et al. 2011, *A&A*, 528, L7
- Kraus, A. L., Ireland, M. J., Martinache, F., & Lloyd, J. P. 2008, *ApJ*, 679, 762
- Kraus, A. L., Ireland, M. J., Martinache, F., & Hillenbrand, L. A. 2011, *ApJ*, 731, 8
- Kraus, A. L., & Ireland, M. J. 2012, *ApJ*, 745, 5
- Kraus, A. L., Ireland, M. J., Hillenbrand, L. A., & Martinache, F. 2012, *ApJ*, 745, 19
- Lacour, S., Tuthill, P., Amico, P., et al. 2011, *A&A*, 532, A72
- Lafrenière, D., Jayawardhana, R., Brandeker, A., Ahmic, M., & van Kerkwijk, M. H. 2008, *ApJ*, 683, 844
- Lenzen, R., Hartung, M., Brandner, W., et al. 2003, *Proc. SPIE*, 4841, 944
- Lubow, S. H., & D'Angelo, G. 2006, *ApJ*, 641, 526
- Luhman, K. L. 2007, *ApJS*, 173, 104
- Manoj, P., Kim, K. H., Furlan, E., et al. 2011, *ApJS*, 193, 11
- Markwardt, C. B. 2009, *Astronomical Data Analysis Software and Systems XVIII*, 411, 251
- Marley, M. S., Fortney, J. J., Hubickyj, O., Bodenheimer, P., & Lissauer, J. J. 2007, *ApJ*, 655, 541
- Martinache, F., Rojas-Ayala, B., Ireland, M. J., Lloyd, J. P., & Tuthill, P. G. 2009, *ApJ*, 695, 1183
- Mathews, G. S., Williams, J. P., & Ménard, F. 2012, *ApJ*, 753, 59
- McClure, M. K., Furlan, E., Manoj, P., et al. 2010, *ApJS*, 188, 75
- Najita, J. R., Strom, S. E., & Muzerolle, J. 2007, *MNRAS*, 378, 369

- Natta, A., Testi, L., Muzerolle, J., et al. 2004, *A&A*, 424, 603
- Nguyen, D. C., Brandeker, A., van Kerkwijk, M. H., & Jayawardhana, R. 2012, *ApJ*, 745, 119
- Olofsson, J., Benisty, M., Augereau, J.-C., et al. 2011, *A&A*, 528, L6
- Pinte, C., Ménard, F., Duchêne, G., & Bastien, P. 2006, *A&A*, 459, 797
- Pott, J.-U., Perrin, M. D., Furlan, E., et al. 2010, *ApJ*, 710, 265
- Pravdo, S. H., Shaklan, S. B., Wiktorowicz, S. J., et al. 2006, *ApJ*, 649, 389
- Siringo, G., Kreysa, E., Kovács, A., et al. 2009, *A&A*, 497, 945
- Skrutskie, M. F., et al. 2006, *AJ*, 131, 1163
- Tatulli, E., Benisty, M., Ménard, F., et al. 2011, *A&A*, 531, A1
- Thalmann, C., Grady, C. A., Goto, M., et al. 2010, *ApJ*, 718, L87
- Tuthill, P., Lacour, S., Amico, P., et al. 2010, *Proc. SPIE*, 7735,
- Whittet, D. C. B., Prusti, T., Franco, G. A. P., et al. 1997, *A&A*, 327, 1194
- Williams, J. P., & Cieza, L. A. 2011, *ARA&A*, 49, 67

Table 1. FL Cha photometry data

Wavelength (μm)	Flux (mJy)	Flux (mag)	Error ^a (mJy)	Telescope	Reference ^b
0.44	1.74E-01	18.44	30%	ground based	1
0.55	1.16E+00	16.28	30%	ground based	1
0.65	3.19E+00	14.96	20%	ground based	1
0.80	1.10E+01	13.41	20%	ground based	1
1.25	5.45E+01	11.73	15%	2MASS	2
1.66	1.17E+02	9.90	15%	2MASS	2
2.20	1.51E+02	9.11	15%	2MASS	2
3.6	9.66E+01	8.66	10%	<i>Spitzer</i>	3
4.5	8.20E+01	8.35	10%	<i>Spitzer</i>	3
5.8	5.60E+01	8.28	10%	<i>Spitzer</i>	3
8.0	3.95E+01	8.02	10%	<i>Spitzer</i>	3
24	1.01E+02	4.67	10%	<i>Spitzer</i>	3
70	3.01E+02	...	15%	<i>Spitzer</i>	3
870	3.00E+01	...	15%	APEX	4

Note. — ^athe optical and near-IR uncertainties are dominated by the extinction corrections. ^bReferences: (1) Gauvin & Strom (1992); (2) Skrutskie et al. (2006); (3) *Spitzer's* Gould Belt Catalog. The 3.6–8.0 μm photometry have already been published by Cieza et al. (2009). The 24 and 70 μm data have not been published before; (4) this work.

Table 2. Disk and Stellar Parameters

Parameter	value	error
Stellar parameters		
Stellar T_{eff} [K]	3850	fixed
Stellar Luminosity [L_{\odot}]	0.4	fixed
Stellar mass [M_{\odot}]	0.6	fixed
Distance [pc]	160	fixed
Inner and outer disk parameters		
Inclination [deg]	60	fixed
Grain size distribution slope, p	-3.5	fixed
a_{min} [μm]	0.005	fixed
a_{max} [μm]	3900	fixed
Surface density exponent, γ	-1	fixed
Flaring exponent, ψ	1.1	fixed
Inner disk parameters		
Scale height at 10 AU $H_{10,inner}$ [AU]	0.16	0.05
$\text{Mass}_{disk,inner}$ [M_{JUP}] ¹	5×10^{-4}	5×10^{-4}
$R_{inner,in}$ [AU]	0.04	0.01
$R_{inner,out}$ [AU]	0.06	0.05
Outer disk parameters		
Scale height at 10 AU $H_{10,outer}$ [AU]	1.2	0.7
$\text{Mass}_{disk,outer}$ [M_{JUP}] ¹	7.5	1.0
$R_{outer,in}$ [AU]	8.3	1.3
$R_{outer,out}$ [AU]	100	fixed

¹Assumes a gas to dust mass ratio of 100.

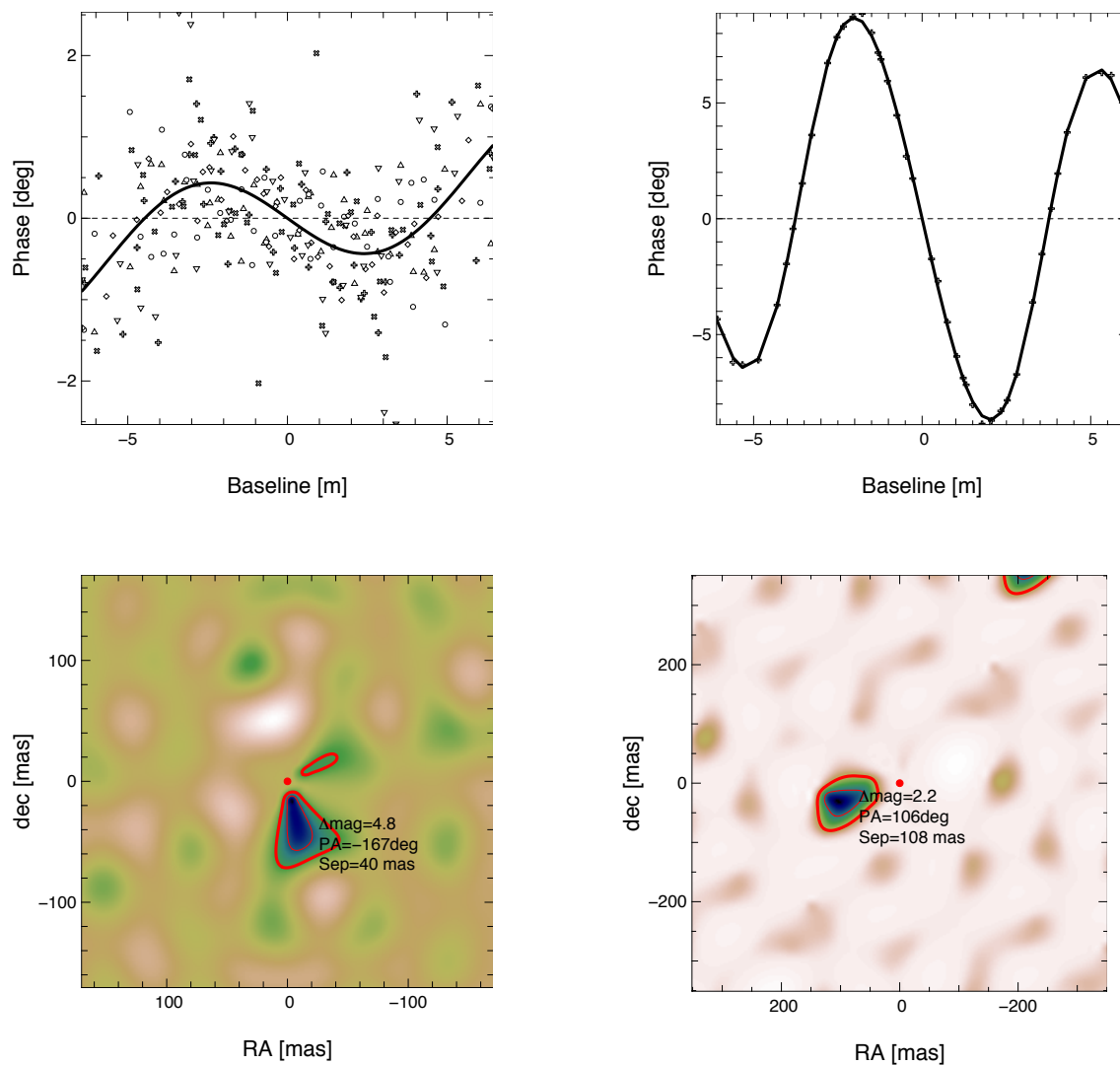


Fig. 1.— **Top Panels:** Closure phase as a function of baseline from our VLT-NACO/SAM data indicating significant flux asymmetries in both FL Cha (left) and RX J1106.3-7721 (right). **Lower Panels:** χ^2 maps resulting from fitting a binary model to the closure phases. The $5\text{-}\sigma$ contours indicate the location of the best-fit companions.

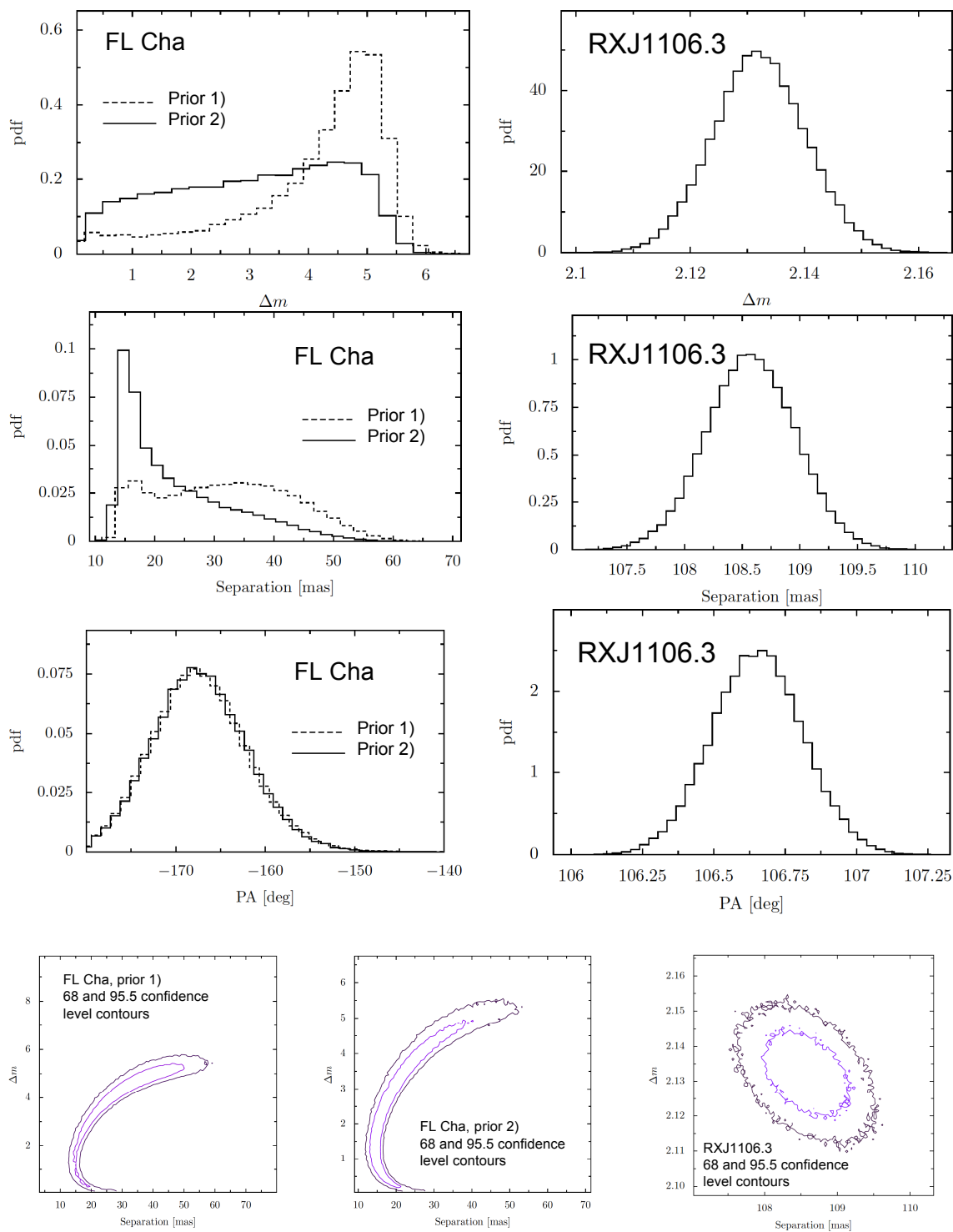


Fig. 2.— **Top Rows:** the posteriori distributions of the 3 parameters in the binary models (Δ mag, separation, and PA) for FL Cha (left, using two sets of priors as described in Section 2.2) and RX J1106.3-7721 (right). **Bottom Row:** The joint distributions of separation and Δ mag. For FL Cha, these two quantities remain degenerate and highly dependent on the choice of priors.

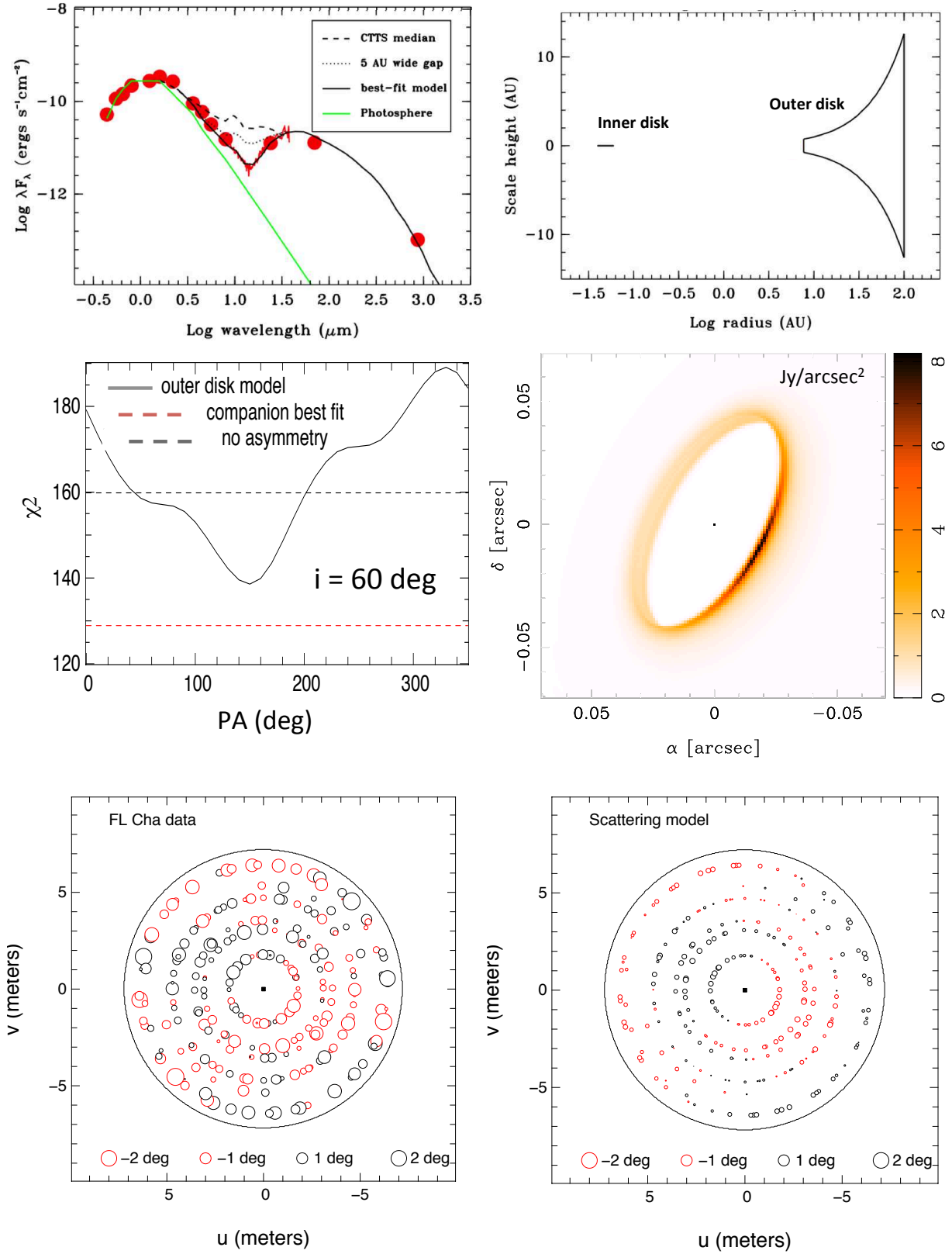


Fig. 3.— **Top Panel:** The extinction-corrected SED of FL Cha showing a pronounced “dip” at mid-IR wavelengths, the defining feature of pre-transitional disks (left) and the disk structure of our best-fit SED model (right). **Middle Panel:** Quality of fit to the SAM data for our best-fit disk model as a function of disk PA, compared to the best-fit binary model and a single point source (left). K_S -band ray traced image of the best-fit disk model (right). **Bottom Panel:** UV coverage of the SAM observations on FL Cha indicating the sign and value of the phases (left). The phases resulting from the best-fit disk model adopting the same UV coverage as in the real data (right).